Earthq Eng & Eng Vib (2013) 12: 155-164 **DOI**: 10.1007/s11803-013-0159-z

Centrifuge modeling of buried continuous pipelines subjected to normal faulting

Majid Moradi†, Mahdi Rojhani‡, Abbas Galandarzadeh† and Shiro Takada*

School of Civil Engineering, College of Engineering, University of Tehran, Iran

Abstract: Seismic ground faulting is the greatest hazard for continuous buried pipelines. Over the years, researchers have attempted to understand pipeline behavior mostly via numerical modeling such as the finite element method. The lack of well-documented field case histories of pipeline failure from seismic ground faulting and the cost and complicated facilities needed for full-scale experimental simulation mean that a centrifuge-based method to determine the behavior of pipelines subjected to faulting is best to verify numerical approaches. This paper presents results from three centrifuge tests designed to investigate continuous buried steel pipeline behavior subjected to normal faulting. The experimental setup and procedure are described and the recorded axial and bending strains induced in a pipeline are presented and compared to those obtained via analytical methods. The influence of factors such as faulting offset, burial depth and pipe diameter on the axial and bending strains of pipes and on ground soil failure and pipeline deformation patterns are also investigated. Finally, the tensile rupture of a pipeline due to normal faulting is investigated.

Keywords: centrifuge models; buried pipeline; normal faulting; earthquake; permanent ground deformation

1 Introduction

Three types of faulting may occur during earthquakes: strike-slip, normal and reverse. The predominant relative motion between sides of a strike-slip fault is horizontal (Fig. 1(a)). However, the predominant relative movement is vertical in normal and reverse faulting. When the hanging side of the fault (right side of Figs. 1(b) and 1(c)) moves downward, the fault is considered to be normal (Fig. 1(b)). When it moves upward, the fault is reverse (Fig. 1(c)).

At times, strike-slip faulting combines with normal or reverse faulting to create oblique faulting. Differential ground movement may result in serious damage from tension or compression on a pipe passing through a fault zone. Hence, faulting is one of the most severe seismic hazards for pipelines. Examples of this include the extensive damage to water transmission lines during the 1906 San Francisco earthquake; damage to pipelines caused by normal faulting during the 1999 Chi-Chi, Taiwan earthquake (O'Rourke and Liu, 1999); leakage from a 2.2 m diameter steel pipe from the Izmit, Turkey earthquake in 1999 caused by strike-slip faulting with a 3 m offset; and the buckling of a water supply pipeline in the 1990 Manjil (Fig. 2), Iran earthquake caused by reverse faulting (Towhata, 2008).

The importance of pipelines as lifelines to communities has prompted extensive research on their response when subjected to faulting. Analytical research was first carried out by Newmark and Hall (1975), Kennedy *et al*. (1977) and Takada *et al*. (2001). Experimental studies were initiated by Audibert and Nyman (1977) and Takada (1984) through the physical modeling of segmental pipelines subjected to normal faulting. Since 2003, large scale and centrifuge-based modeling of pipelines subjected to faulting has been carried out by O'Rourke *et al*. (2005).

Most of these works were designed to assess pipe response to strike-slip faulting and some were implemented to recognize the behavior of pipelines under normal faulting with right deformation angles. Some of these studies were conducted by Yoshizaki *et al*. (2001) in U.S.-Japan cooperative research. However, several numerical studies were also conducted during this same time period. Ariman and Lee (1991) evaluated pipe strain using a finite element model in 1991, where the effects of pipe diameter, burial depth and soil friction were studied on pipe bending strain. Meyersohn (1991) investigated pipe strain using Unipip finite element software. Liu and O'Rourke (1997) implemented numerical and analytical research on the behavior of a continuous pipeline in 1997.

Experimental, analytical or numerical research on pipeline response due to normal and reverse faulting

Correspondence to: Majid Moradi, Department of Soil Mechanics and Foundation Engineering, School of Civil Engineering, University of Tehran, Iran
Tel: +982122783472; Fax: +982122783492
E-mail: mmoradi@ut.ac.ir
†Assistant Professor; ‡PhD Candidate; §Adjunct Professor
Received September 7, 2011; **Accepted** November 8, 2012

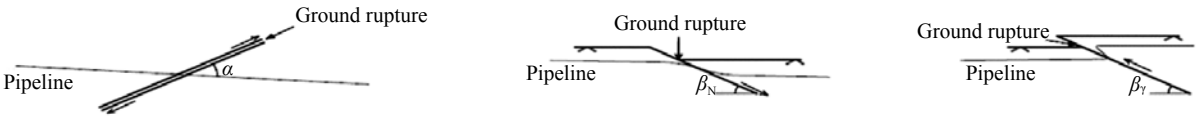

(a) Strike-slip fault (b) Normal fault (c) Reverse fault

Fig. 1 Fault types

Fig. 2 Pipeline damaged by reverse faulting during 1990 Manjil, Iran earthquake (courtesy of Prof. Towhata)

has been limited. Furthermore, the results of analytical or numerical studies should be verified by case histories. Because of the lack of validated case histories, centrifuge-based modeling of the buried pipeline response to fault offset is the best approach to verify and calibrate analytical and numerical results and also to characterize pipeline behavior under faulting (Ha *et al*., 2008).

The present research project on centrifuge modeling of buried pipelines subject to faulting was planned and implemented at the physical modeling and centrifuge laboratory of the Soil Mechanics and Foundation Engineering Department at the University of Tehran. A fault simulator was designed and constructed to simulate normal and reverse faulting to study its impact on the behavior of continuous steel pipes. Pipe response to reverse faulting and details of the fault simulator have been presented elsewhere by the authors (Rojhani *et al.*, 2011a, 2011b, 2012a, and 2012b).

2 Modeling equipment and preparation

Table 1 summarizes three centrifuge experiments designed to study the behavior of a buried pipeline subjected to normal faulting. All centrifuge tests were carried out at a gravity level of 40 g and with 2.3 m peak fault offset. The pipe-fault angle was 90° and the deformation angle of the fault was 60° for all tests. The 8 mm diameter pipes corresponded to 0.32 m in the prototype. A diameter to thickness ratio of 20 was used for tests 1 and 2. In Test 3, the pipe with 25 mm diameter corresponds to 1.0 m in the prototype when a *D/t* ratio of 50 was used. The ratios of burial depth to diameter of pipe were 2.8, 6, and 2 in Tests 1, 2, and 3, respectively. The relation between the parameters in the model and the prototype are shown in Table 2.

2.1 Fault simulator specifications

The simulator at the University of Tehran (FSUT-RN 60.8) is made of aluminum alloy. The outer dimensions are 102 cm in length, 76 cm in width, 68 cm in height and 2300 N in weight. The soil split container is 96 cm in length, 70 cm in width and 23 cm in height. The normal deformation angle of the fault in FSUT-RN 60.8 is 60° (β = 60°). The faulting plane divides the container into two unequal halves with the larger half being movable and the smaller half fixed. The maximum allowable offset of the simulator is ±4 cm, simulating ±2 m offset at 50 g.

A wedge-like mechanism is used in the driving system to increase the stability of the movable half and increase the accuracy and tolerance of asymmetric forces during the test. The driving force is provided by a 50 kN hydraulic jack placed horizontally under the soil container. This hydraulic actuator shifts the wedge-like driving component in and out under the movable half.

In spite of the capability for offset rate control, in

Table 1 Summary of test models used in centrifuge testing (all dimensions in prototype scale)

Test No.	Test label	*D* (m)	*t* (mm)	*D/t*	H (m)	*H/D*	β(°)	α(°)	Acc. (g)	Peak offset (m)
1	8S4N-2.8S	0.32	16	20	0.88	2.8	60	90	40	2.3
2	8S4N-6S	0.32	16	20	1.90	6.0	60	90	40	2.3
3	25S5N-2S	1.00	20	50	2.00	2.0	60	90	40	2.3

this series of tests, the simulator ran at the maximum rate. On the prototype scale, the maximum offset rate of FSUT-RN 60.8 is 20 cm/s for normal faulting.

2.2 Soil and pipe specifications

Test model specifications are shown in Table 1. All tests were conducted on stainless steel-316 pipes that complied with ASTM standard A999/A999M. The pipe-fault angle—the angle between the pipe axis and fault direction in a planar view—was 90° in all tests. The pipeline was connected to the simulator end walls using fixed connections. The pipe was welded to a bolted rod at the ends using oxy-acetylene gas and then the ends of the bolted rods were fastened to the simulator end walls using nuts (Fig. 4).

To simulate realistic field end conditions on pipelines and avoid the effect of pipe end conditions on pipe response, a length of complete pipeline affected by faulting should be modeled. The affected length of pipeline was located between the two anchored points.

Table 2 Scaling laws for centrifuge testing

Parameter	Model\ Prototype	Dimensions
Length	$1/N$	L
Strain	1	1
Stress	1	$ML^{-1}T^{-2}$
Acceleration	N	LT^{-2}
Axial rigidity	$1/N^2$	MLT^{-2}
Flexural rigidity	$1/N^4$	ML^3T^{-2}

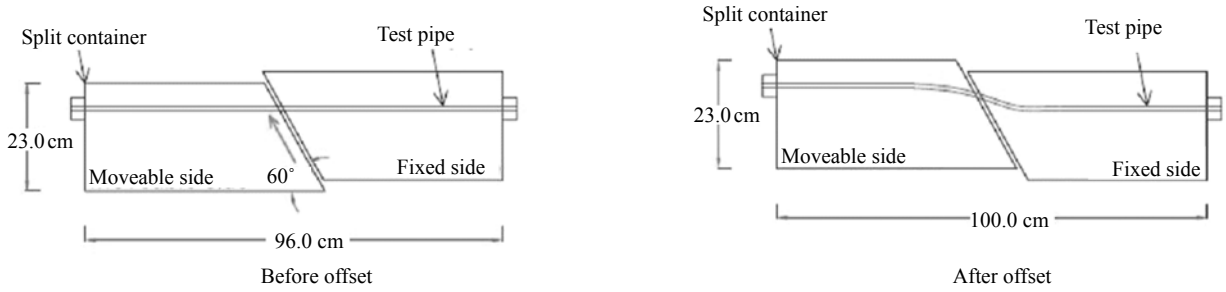

Elevation view of 60° normal faulting test setup

Fig. 3 Components of University of Tehran fault simulator (FSUT-RN 60.8)

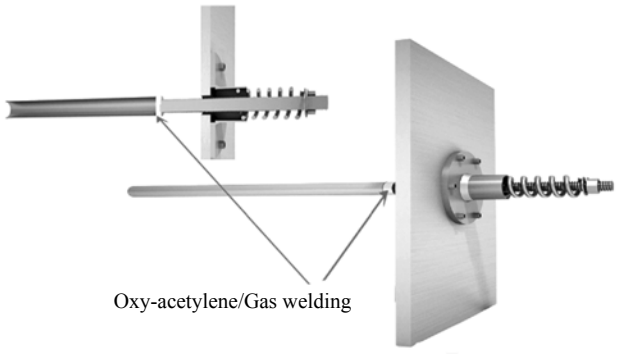

Fig. 4 Pipe end connector to fault simulator body

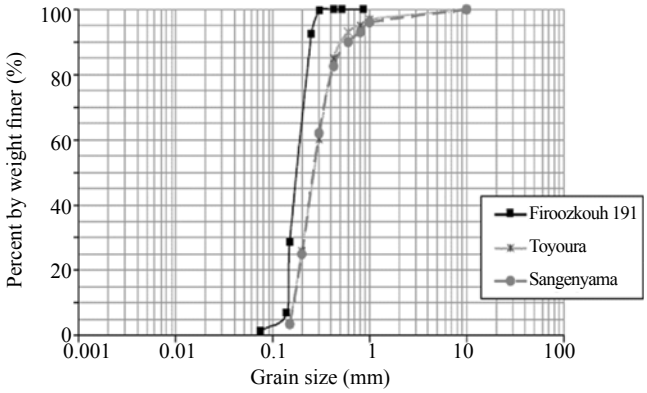

Fig. 5 Grain size distribution of Firoozkouh-191 sand

These anchor points were assumed to be the last affected points of the pipeline subject to faulting and were located on the two sides of the fault. However, since there is no precise method to estimate the exact affected length of a pipeline or the distance between the two anchored points, it was roughly analytically estimated at 70–80 m. Based on the scaling laws in the centrifuge, a modeled pipe 1 m in length at 40 g will equal a 40 m pipeline on the prototype scale. Thus, model response is affected by boundary conditions.

When it is not possible to model the entire affected length of a pipeline, the boundary condition of the modeled pipeline will affect pipe response and the pipe end connection will be significant. For such models, the pipe-end condition should be semi-rigid, meaning that it is neither a fully-fixed nor a fully-hinged joint. The pipe is neither fixed, without deformation, nor free, because resistance of the remaining part of the pipe prevents free deformation. Since the rate of pipe deformation at the end of the pipe model is unknown, simulation of a semi-rigid joint is not possible. However, realistic pipe behavior can be understood by considering the limit boundary conditions of fully-fixed and fully-hinged cases. Fixed connections were modeled in this study because they are most likely to simulate real conditions. However, modeling a pipeline with a pin connection is necessary and recommended for future research.

Grain size of the soil is another important factor affecting the results of soil-structure interaction in centrifuge modeling. The soil used in this study was Firoozkouh 191 sand. Its grain size curve is shown in Fig. 5. The G_s factor of this sand was 2.65 and the average grain size diameter (D_{50}) was 0.16 mm. Therefore, the smallest ratio of pipe diameter to average soil grain size (D/D_{50}) was 50, which satisfied the criterion of $OD/D_{50} \geq 48$ recommended by TC2 based on centrifuge test data from Ovesen (1981) and Dickin and Leuoy (1983). The properties of the Firoozkouh-191 sand shown in Table 3 are the specific gravity of soil particles, maximum and minimum void ratios, average particle size, fine content of the soil, coefficient of uniformity and curvature. In Table 3, the properties of Toyoura and Sengenyama sands are also presented for comparison purposes with the Firoozkouh-191 sand.

The soil moisture content was assumed to be 4.5%–5%, which replicated the expected pipe burial condition. Moist soil was placed inside the soil container in 4 cm layers, then compacted using a steel compactor (width = 18.2 cm, length = 24.7 cm, weight = 19.1 N) with a dropping height of 10 cm and 10 replications. The input energy was about 425 J/m^2 and resulted in about 85% relative soil density. As done for the prototype, the pipe was placed in a trench. The soil container was filled with compacted soil and a trench was excavated in it. The pipe was then placed into the trench and all the extracted soil was piled over the pipe.

Steel pipelines usually have a polymer coating. The significant role of the friction coefficient between the soil and the pipe in pipe response was approximated by coating the pipe model with a polymer tape. The coating also protected the strain gauges during the test. Such a coating should increase the friction between the soil and the pipe due to the sinking of soil particles.

Table 3 Properties of Firoozkouh-191, Toyoura and Sengenyama sands

Sand type	G_s	e_{max}	e_{min}	D_{50} (mm)	FC	C_u	C_c
Firoozkouh-191	2.65	0.894	0.622	0.17	1%	1.27	.96
Toyoura	2.65	0.977	0.597	0.17	0%	1.54	1.25
Sengenyama	2.72	0.911	0.55	0.27	2.3%	2.15	1.21

* Ghalandarzadeh (1997)

2.3 Instrumentation

In these tests, strain gauges and displacement transducers were used to monitor the response of a pipeline subject to faulting.

Twenty-six strain gauges were arranged at seven stations along the pipeline length and installed in a longitudinal and circumferential arrangement on the pipe. On parts of the pipe where large deformation was expected, the type of strain gauge was changed to measure the large strain of ±20%. All strain gauges were set in a quarter bridge configuration to allow separation of axial strain from bending strain along the pipeline.

Six displacement transducers measured any deformations occurring in the model. One measured fault displacement, two measured axial deformation at the two ends and three measured the vertical displacement of the pipe (Fig. 6). Sampling speed throughout the test was considered to be 50 Hz.

A colored marker network was used at the soil surface to delineate surface deformations. Colored sand layers were used to mark any deformation and displacement in depth.

3 Discussion and results

3.1 Post-offset ground surface and pipe deformations

Ground surface, section and pipeline deformations near the fault are shown in Figs. 7–9. Note that the observed ground surface deformation and longitudinal and transverse cracks on the fault zone are similar in all three tests, except at the intersection of the pipeline and fault trace. Soil subsidence was clearly visible at this intersection. The differences are shown in Fig. 7. Where the burial depth to the pipe diameter ratio (*H/D*) was higher, soil disturbance and observed failure decreased. The ground surface on the up-thrown, or footwall, side showed little deformation, because the pipeline on this side moved down and the top soil remained undisturbed by the arching mechanism. Where *H/D* ratio was lower, conical masses of soil were thrown up near the pipe end connection. This may have been caused by the rupture and release of sudden stresses on the pipe.

During the test, the pipeline moved upward on the hanging wall side, as shown in Fig. 7. The pipe plowed through the soil and in some places was exposed at the surface. It is clear that, by increasing the pipe diameter and decreasing the burial depth, soil disturbance along the pipe axis increased and the cracks became larger. Some transverse cracks perpendicular to the pipe axis also occurred on the hanging wall side, which was probably due to soil shear failure caused by faulting.

As shown in Figs. 8–9, pipe rupture occurred when the pipeline was subjected to tension. In all tests, rupture points along the pipe were similar and occurred adjacent to the pipe end connection on the footwall side. These results will be discussed below. As shown in Fig. 9, the displacement after rupture on the free end of the pipe buried at a shallow depth was larger than for the more deeply buried pipelines.

3.2 Axial strain

Figures 10 and 11, respectively, show the measured axial strain and bending strain along the pipe during faulting. The highest offset applied during the tests was 2.4 m on the prototype scale. However, only those results obtained before pipe rupture were considered to be valid and are presented. Because the pipe rupture disturbed some strain gauges, results obtained after the rupture were not considered reliable. The figure legends show the faulting offset at which the pipe ruptured as well as the pipe diameters and *H/D* ratios. The curves

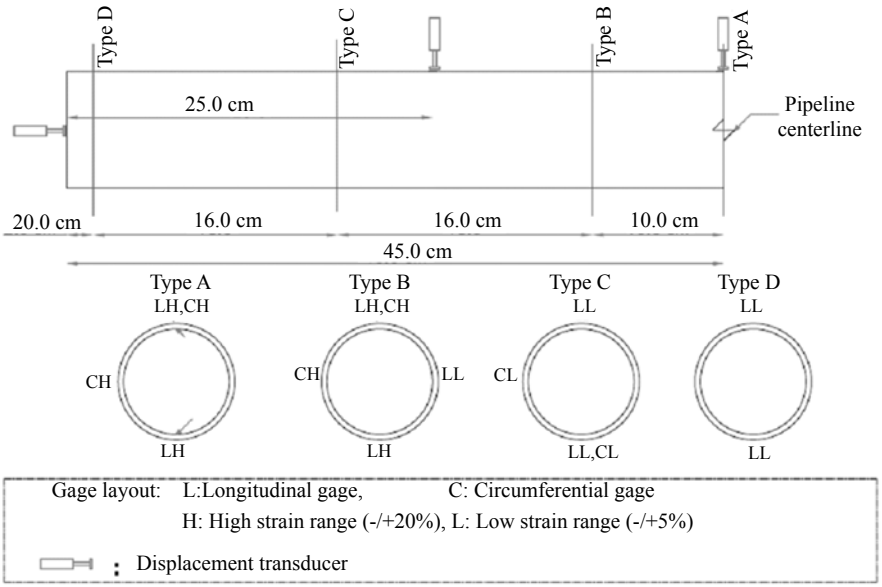

Fig. 6 Arrangement of strain gauges and displacement transducer along the pipe

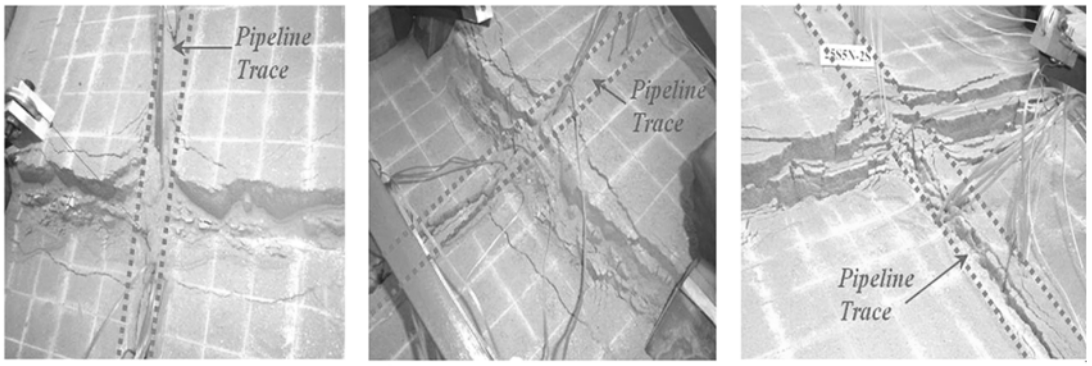

(a) Test-1 (b) Test-2 (c) Test-3

Fig. 7 Post-test surface observations

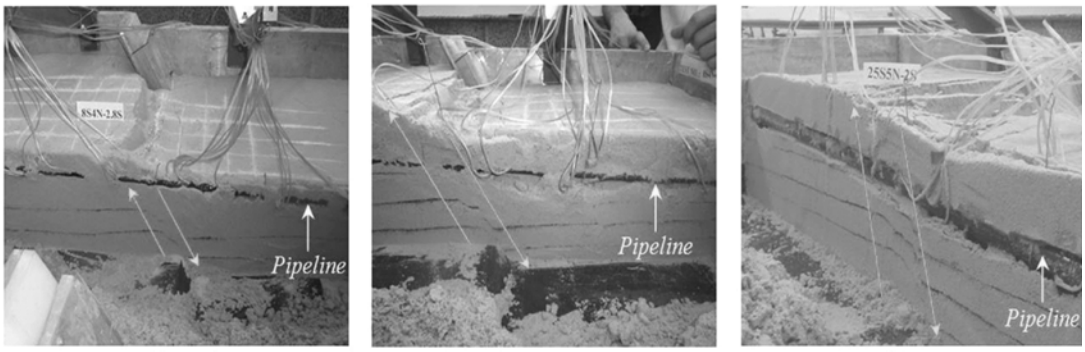

(a) Test-1 (b) Test-2 (c) Test-3

Fig. 8 Post-test pipeline and soil section deformation

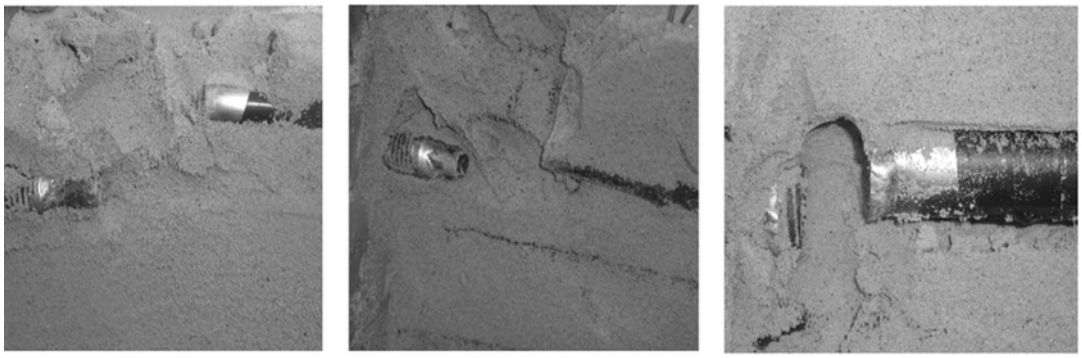

(a) Test-1 (b) Test-2 (c) Test-3

Fig. 9 Rupture of pipeline during faulting

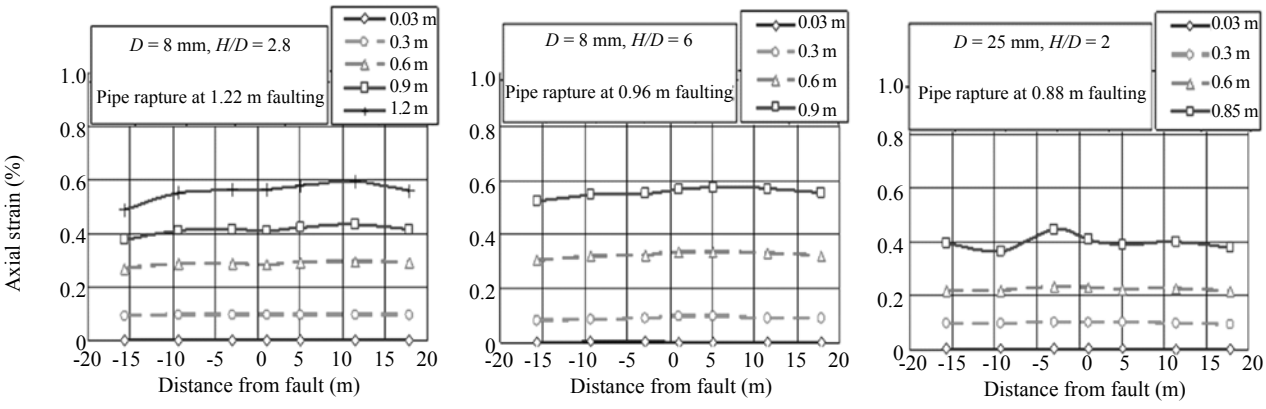

(a) Test-1 (b) Test-2 (c) Test-3

Fig. 10 Axial strains at various offsets, variation with distance from fault

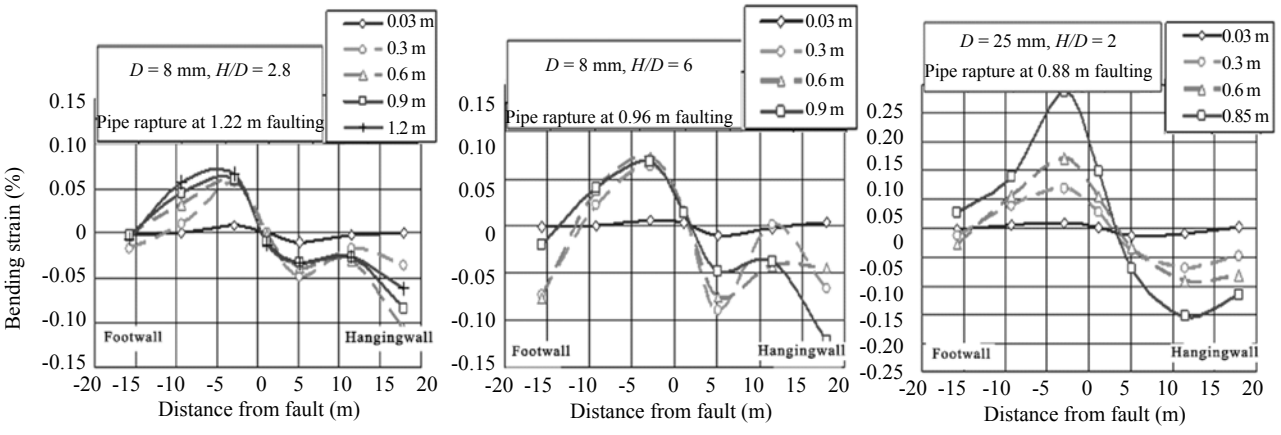

(a) Test-1 (b) Test-2 (c) Test-3

Fig. 11 Bending strains at various offsets, variation with distance from fault

in these figures correspond to the offsets specified in the legend.

As shown in Figs. 10 and 11, the axial strain was greater than the bending strain and did not significantly change along the length of the pipeline. The 60° deformation angle of the simulated fault resulted in considerable axial tension along the pipe. The peak axial strain for all tests was at the intersection of the fault and the pipe at ±10 m from the fault. Beyond this, the axial strain decreases linearly as the distance from the fault increases. This is consistent with the constant longitudinal friction force per unit length at the soil-pipe interface.

As expected from the faulting geometry, the axial strain curve is asymmetric. The asymmetry of the strain curve is greater near the fault (±10 m from the fault) and beyond this it became symmetric. Figure 10(c) shows that, at large offsets, some variation is visible in the curve on the footwall side. This is due to cracking or local ruptures that occurred before the complete rupture of the pipe.

The pipe axial strain on the hanging wall side as shown in Fig. 10 is always larger than that on the footwall side. This may have arisen from the different friction forces per unit length at the soil-pipe interface on the footwall and hanging wall sides. The friction force per unit length is constant on the footwall and the hanging wall sides, but is not the same for the two sides. On the footwall side, the pipe moved downward and rested in full contact with the soil bed, which caused the friction force at the soil-pipe interface to increase. Thus, the axial strain decreases more rapidly on the footwall side. This difference in the soil–pipe friction force of the two sides may be another reason for the change in axial strain by increasing the faulting offset and its asymmetry.

As shown in Fig. 10, the pipe axial strain increases as the pipe burial depth increases. The deeper the burial depth was, the lower the fault offset at which the pipeline ruptured. However, at small offsets, the axial strain at the deeper burial depths is slightly higher than at shallow depths. As the fault offset increases, the difference becomes prominent. The overall effect of increasing the pipe burial depth is to reverse the pipe rupture fault offset. Increasing the burial depth decreased the fault offset to pipe rupture. As expected, the strain at the rupture point in all tests is almost constant because the rupture strain of pipe is affected by the material properties of the pipe.

Figure 12 plots the peak axial strains of the pipe versus the fault offsets. Note that peak axial strain versus fault offset for all three tests follows nearly the same curve although the variation of burial depth affects the axial strains. In other words, it seems that for similar faulting offsets, pipes buried at shallow depths experience fewer strains when compared to pipes buried at greater depths. The results also showed that pipes with larger diameter were subjected to relatively higher strains at low offsets. Figure 12 shows the axial strain rate increases less in pipe with larger diameter than in pipes with smaller diameters.

Figure 12 also shows the estimated peak axial strain based on Kennedy's analytical method (1977). Note that the peak axial strain is significantly underestimated.

According to Newmark and Hall (1975), the yield strain of a pipe is 4%. Based on Kennedy's model (1977), the maximum allowable tensional strain is 2%–5%. The question arises as to why the tested pipes ruptured at low strains of less than 1%. This issue will be answered after bending strains are studied.

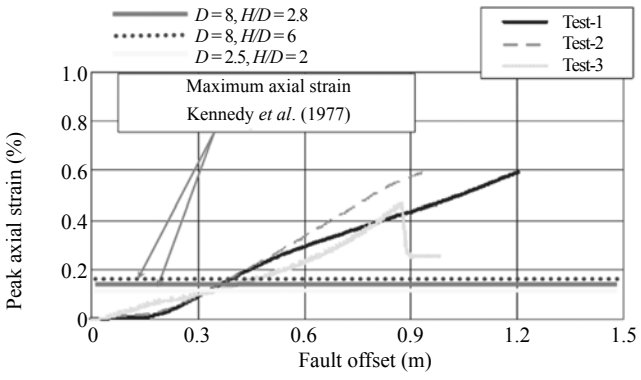

Fig. 12 Peak axial strain versus fault offset

3.3 Bending strain

Bending strain along the pipeline during faulting is shown in Fig. 11. It can be observed that the bending strain curve along the pipe subjected to normal faulting with 60° deformation is asymmetric with double curvature. The convexity of the curve is on the footwall side and its concavity is on the hanging wall side. At low offset faulting, the bending strain values on the footwall side are lower than on the hanging wall side. It seems that in the elastic strain range, the difference between soil stiffness below and above the pipe resulted in different strains on the two sides. A gradual increase in faulting offset resulted in more rapidly increasing pipe bending strains near the fault. Thus, the bending strain curve reaches a peak at ±5 m from the fault.

As shown in Fig. 11, the bending strain curve on the footwall side is uniform, but on the hanging wall side, it is non-uniform and step-like. On the footwall side, the bending axis of the pipe due to faulting is the same as the bending axis from soil overburden. The opposite trend is seen on the hanging wall side.

The mobilization of bending moment at the end connections of the pipe may be another reason for such a pattern in the bending strain curve on the hanging wall side. Since the pipe was connected to the simulator body using a fixed joint, the end of the pipe may have attracted the moment, subjecting the pipe to considerable bending moment near the end connection on the hanging wall side. Under these conditions, the resultant bending strain curve becomes similar to Fig. 11. Also, the pipe end connection may have been subjected to bending moment on the footwall side. For pipes at shallow burial depths, the considerable bending strain on the pipe end connection was not recorded for the footwall side, while pipes buried more deeply were subjected to bending strain at the end on the footwall side.

Figure 11 also shows that at increasing pipe burial depths, the strain curve becomes step-like where pipe diameter is constant. The bending strain curve of pipes with larger diameters and more relative stiffness does not show this pattern.

Figure 13 shows the maximum bending strain changes along the footwall and hanging walls. As observed, the bending strain along the footwall does not vary much by depth. However, an increase in pipe diameter results in a considerable increase of bending strain along the footwall. According to the measured strains, the variation of maximum bending strain along the hanging wall side is uniform. The maximum strain curve is affected by pipe diameter and burial depth.

Figure 13 also shows the maximum bending strain estimated based on Kennedy's analytical equation (1977). Contrary to the axial strain, it seems that bending strain has been overestimated, but this is not certain since the rupture that occurred on the pipe prevented an increase in the bending strain.

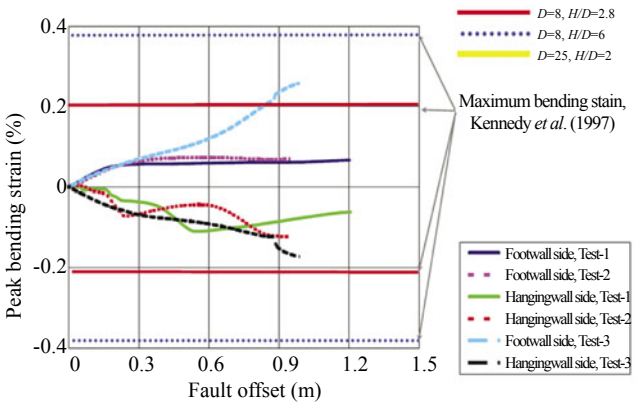

Fig. 13 Peak bending strain versus fault offset

3.4 Vertical displacement along pipe

Figure 14 shows the vertical displacement along the pipe measured by three displacement sensors. One sensor was installed at the middle of the pipeline and other two on each side of the fault at 8 m on the prototype scale. Note that the recorded displacement at the middle of the pipe is similar for all tests from the beginning of deformation and for its gradient. This may have been caused by soil disturbances at the fault-pipe intersection.

Pipe vertical displacement along the sides of the fault depends on burial depth. In shallow conditions, displacement along the footwall starts at ±0.4 m offset. Along the hanging wall side, the pipe shows little displacement up to 0.5 m offset and afterward displacement becomes constant. As expected, increasing burial depth results in no displacement up to 0.6 m offset.

Increasing pipe diameter causes the vertical displacement of the pipe to begin earlier and at a low offset resulting from a decrease in pipe flexibility. In other words, when pipe stiffness increases, faulting impact on the other parts of the pipe is greater and more rapid. It should be noted that the fall at the end of the displacement curve is caused by pipe rupture.

3.5 Pipe rupture

It was observed that the test pipes encountered a rupture adjacent to the pipe connector on the footwall side. Pipelines that were more flexible (smaller diameter) and buried in softer soil (shallow depth) showed more capability to deform before rupturing. Thus, failure occurred at greater faulting offsets. Although the pipe rupture occurred at less than 1% strain, the rupture strain determined by Newmark and Hall (1975) is about 4%.

The type of end connector was the main reason for the rupture of the pipe. Slip joints with oxy-acetylene/gas were used to connect the pipe and end connector. This type of joint does not support high tensional strain and usually reaches the rupture point before the failure of the pipe itself. The results showed that the rupture occurred

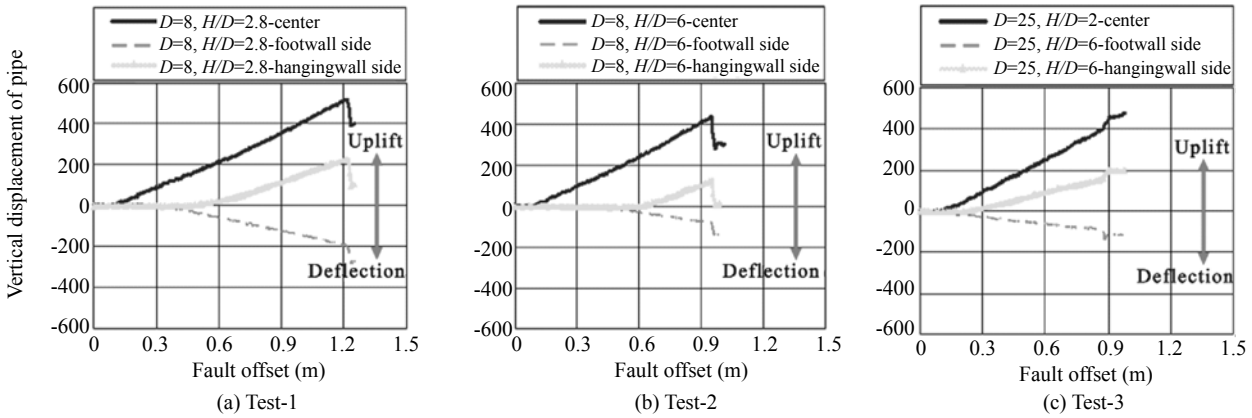

Fig. 14 Vertical displacement along the pipe

at the end of the pipe, while the maximum strain usually occurs adjacent to the fault. This indicates a defect at the rupture point as the cause of the rupture. Studies have been conducted by Tawfik and O'Rourke (1985), Moncarz *et al*. (1987) and Brockenbrough (1990) in this area. Tawfik and O'Rourke (1985) presented the efficiency of slip joints with external welding similar to the joints used in this study. According to their results, the maximum efficiency of oxy-acetylene/gas welding joints in these tests is 0.29. In other words, the joint strength for the three tests is, at most, 29% of pipe strength. This coefficient is only suitable for welded joints with no defects such as porosity or gaps.

Other types of welding were not possible in this study because of the very thin wall thickness of the pipe. The presence of gas-welded joints along the pipe was the main weakness that led to rupture earlier than expected.

4 Conclusions

Three centrifuge tests were conducted to investigate the behavior of a buried steel pipeline subjected to normal faulting. Stainless steel pipes with different diameters were used in all the tests and connected to the simulator box by a fixed connector buried at two different depths. The deformation angle of the fault in all tests was 60°. Axial strains, bending strains and vertical displacements caused by faulting were measured. From the tests, the following conclusions can be drawn:

The greatest strains caused by pipe deformation were axial strains that were 2–10 times greater than bending strains. While axial strain was the prevailing strain occurring along the pipe, as pipe diameter increased, bending strain also increased and approached the axial strain. Thus, it appears that axial deformation caused by normal faulting was the main reason for pipe rupture.

Since pipe rupture was the result of axial and bending strains and strain patterns developed along the pipe, it seems that when the pipes lack weak points such as welded joints, the rupture point is located at a point 10–15 times the pipe diameter from the fault.

Welded oxy-acetylene/gas type joints caused premature rupture along the pipe, even in low strain cases. In these tests, connector resistance equaled 20% of pipe resistance. The welded joint ruptured when the strain reached 0.20 times the tolerable strain of the pipe.

Pipe burial depth and diameter did not significantly influence pipe rupture. The pipe was subjected to rupture due to axial strain caused by deformation.

Increasing the burial depth resulted in increased soil stiffness around the pipe and increased pipe diameter resulted in rupture occurring at lower faulting offsets. Thus, reducing soil overburden by using light weight gravel or EPS backfill instead of soil may decrease the effective stress of the soil, decrease soil stiffness and increase the tolerance of the pipe offset. Increasing the pipe diameter also increased the bending performance of the pipe and decreased its axial performance.

It was observed that the maximum axial strain of the pipe was subjected to a linear increase as faulting increased. These results indicate that Kennedy's analytical method (1977) underestimates the maximum axial strain.

The results also showed that greater burial depth delayed pipe exposure at the soil surface, but increased pipe diameter expedited pipe exposure at the surface.

Conducting similar tests using pipes with pin connections is suggested, because the realistic behavior of the pipeline lies between the two model responses of fixed and pin connections. Further tests are also needed to model the effect of internal pipe pressure.

Acknowledgment

This work was conducted at the Physical Modeling and Centrifuge Laboratory of the Soil Mechanics and Foundation Engineering Department in the School of Civil Engineering, University of Tehran. The authors express their deep gratitude to all experts and personnel of the lab, especially Mr. Ebrahimi, Mr. Jabarzade and Mr. Pirnazari for their constructive critiques and assistance.

References

Ariman T and Lee BJ (1991), "Tension/Bending Behavior of Buried Pipelines under Large Ground Deformation in Active Faults," *Proceedings, 3rd US Conference on Lifeline Earthquake Engineering*; Technical Council on Lifeline Earthquake Engineering; ASCE Monograph, **4**: 226–233.

Audibert JME and Nyman KJ (1977), "Soil Restraint Against Hhorizontal Motion of Pipes", *ASCE J Geotechnical Engineering Division*, **103**(GT10): 1119–1142.

Brockenbrough RL (1990), "Strength of Bell-and-spigot Joints", *J. Structural Engineering*, **116**(7): 1983–1991.

Dickin EA and Leuoy CF. (1983), "Centrifuge Model Tests on Vertical Anchor Plates," *ASCE J Geotechnical Engineering*, **109**(12): 1503–1525.

Ghalandarzadeh A (1997), "Shaking Table Tests on Seismic Displacement of Water-front Structures," *PhD Dissertation*, University of Tokyo, Japan.

Ha D, Abdoun TH, O'Rourke MJ, Symans M, O'Rourke TD, Palmer MC and Stewart HE (2008), "Centrifuge Modeling of Earthquake Effects on Buried High-density Polyethylene (HDPE) Pipelines Crossing Fault Zone," *ASCE J Geotechnical and Geoenvironmental Engineering*, **134**: 1501–1515.

Kennedy RP, Chow AW and Williamson RA (1977), "Fault Movement Effects on Buried Oil Pipeline," *ASCE J. Transportation Engineering Division*,**103**(TE5): 617–633.

Liu X and O'Rourke MJ (1997), "Behaviour of Continuous Pipeline Subject to Transverse PGD," *Earthquake Engineering and Structural Dynamics*, **26**: 989-–1003.

Meyersohn WD (1991), "Analytical and Design Considerations for the Seismic Response of Buried Pipelines," *Graduate thesis*, Cornell University.

Moncarz PD, Shyne JC and Derbalian GK (1987), "Failure of 108-inch Steel Pipe Water Main," *ASCE J Performance of Construction Facilities*, **1**(3): 168–187.

Newmark NM and Hall WJ (1975), "Pipeline Design to Resist Large Fault Displacement," *Proceedings, US National Conference on Earthquake Engineering*, Ann Arbor, Michigan; Paper UILU-ENG-75-2011: 416–425.

O'Rourke M, Gadicherla V and Abdoun T (2005), "Centrifuge Modeling of PGD Response of Buried Pipe," *Earthquake Engineering and Engineering Vibration*; **4**(1): 69–73.

O'Rourke M and Liu X (1999), *Response of Buried Pipelines Subject to Earthquake Effects*, Multidisciplinary Center for Earthquake Engineering Research (MCEER), *Monograph Series*, pp. 250.

Ovesen NK (1981), "Centrifuge Tests of the Uplift Capacity of Anchors", *Proceedings, 10th International Conference on Soil Mechanics and Foundation Engineering*, Stockholm, Sweden, pp.717–722.

Rojhani M, Moradi M, Galandarzadeh A and Takada S (2011a), "Centrifuge Modeling of Buried Pipelines Response due to Reverse Faulting," *Proceedings, 5th international Conference on Earthquake Geotechnical Engineering,* Santiago, Chile, Paper No. CMBRO.

Rojhani M, Moradi M, Galandarzadeh A and Takada S (2011b), "Centrifuge Modeling of Buried Pipelines Response due to Normal Faulting," *Proceedings, 14th Asian Regional Conference on Soil Mechanics and Geotechnical Engineering,* Hong Kong, China, Paper No. 188.

Rojhani M, Moradi M, Ebrahimi MH, Galandarzadeh A and Takada S (2012a), "Recent Developments in Faulting Simulators for Geotechnical Centrifuges," *Geotechnical Testing Journal*, ASTM, **35**(6). (In press)

Rojhani M, Moradi M, Galandarzadeh A and Takada S (2012b), "Centrifuge Modeling of Buried Continuous Pipelines Subjected to Reverse Faulting," *Canadian Geotechnical Journal*, **49**(6): 659–670.

Takada S (1984), "Model Analysis and Experimental Study on Mechanical Behavior of Buried Ductile Iron Pipeline Subjected to Large Ground Deformation," *Proceedings, 8th World Conference on Earthquake Engineering*, San Francisco; Vol 7, 255–262.

Takada S, Hassani N and Fukuda K (2001), "A New Proposal for Simplified Design of Buried Steel Pipes Crossing Activ e Faults," *Earthquake Engineering and Structural Dynamics*, **30**: 1243–1257.

Tawfik MS and O'Rourke TD (1985), "Load-carrying Capacity of Welded Slip Joints," *J Pressure Vessel Technology*, **107**: 37–43.

Towhata I (2008), *Geotechnical Earthquake Engineering*, Springer.

Yoshizaki K, O'Rourke TD, Bond T, Mason J and Hamada M (2001), "Large Scale Experiments of Permanent Ground Deformation Effects on Steel Pipelines," http://mceer.buffalo.edu/publications/resaccom/01-sp01/rpa_pdfs/03orourke_tkyogas.pdf [25 May 2011].

List of symbols

C_C = coefficient of curvature
C_u = coefficient of uniformity
D = pipe outer diameter
D_{50} = average particle size of sand backfill
e_{max} = maximum void ratio
e_{min} = minimum void ratio
FC = fine content of soil
G_s = specific gravity of soil particle
H = depth of soil from the surface to the top of pipe
R_0 = pipe radius
t = pipe wall thickness
α = pipeline fault orientation angle
β = fault deformation (dip) angle
EPS = expanded polystyrene